NAVAL POSTGRADUATE SCHOOL

MONTEREY, CALIFORNIA

THESIS

THE INFLUENCE OF BOUNDARY-LAYER SHEAR AND STATIC STABILITY ON LOW-LEVEL VERTICAL ACCELERATIONS IN A SUPERCELL

by

Sean P. Caulfield

December 2018

Thesis Advisor: John M. Peters
Second Reader: Qing Wang

THIS PAGE INTENTIONALLY LEFT BLANK

REPORT DOCUMENTATION PAGE	*Form Approved OMB No. 0704-0188*

1. AGENCY USE ONLY *(Leave blank)*	**2. REPORT DATE** December 2018	**3. REPORT TYPE AND DATES COVERED** Master's thesis

4. TITLE AND SUBTITLE
THE INFLUENCE OF BOUNDARY-LAYER SHEAR AND STATIC STABILITY ON LOW-LEVEL VERTICAL ACCELERATIONS IN A SUPERCELL

5. FUNDING NUMBERS

6. AUTHOR(S) Sean P. Caulfield

7. PERFORMING ORGANIZATION NAME(S) AND ADDRESS(ES)
Naval Postgraduate School
Monterey, CA 93943-5000

8. PERFORMING ORGANIZATION REPORT NUMBER

9. SPONSORING / MONITORING AGENCY NAME(S) AND ADDRESS(ES)
N/A

10. SPONSORING / MONITORING AGENCY REPORT NUMBER

11. SUPPLEMENTARY NOTES The views expressed in this thesis are those of the author and do not reflect the official policy or position of the Department of Defense or the U.S. Government.

12a. DISTRIBUTION / AVAILABILITY STATEMENT
Approved for public release. Distribution is unlimited.

12b. DISTRIBUTION CODE
A

13. ABSTRACT (maximum 200 words)

It is well documented that tornadoes are formed from a special breed of rotating thunderstorms called supercells, and that tornadogenesis is a result of several factors, one of which is the vertical stretching of low-level vorticity. Not as well understood are the factors that contribute to vertical acceleration of low-level vorticity in the updraft region of a supercell to support tornadogenesis. This paper examined the influence of combining both low-level shear and low-level static stability on low-level vertical accelerations using idealized simulation from Cloud Model 1 (CM1). A matrix of simulations varied the low-level shear and the low-level convective inhibition (CIN) in order to parse out the dynamic response of these parameters on the low-level forcing. When shear was added to simulations, there was a consistent positive response to the low-level dynamic forcing; when low-level CIN was increased, there was a consistent negative response to the low-level buoyant forcing. Despite the chaotic nature of a supercell environment, a balance can be achieved in the lower atmosphere where the low-level CIN can counteract the low-level shear and inhibit the vertical stretching of vorticity. Since this phenomenon is associated with tornadogenesis, a correlation can be made between the ratio of low-level static stability to low-level shear and its effect on tornado formation.

14. SUBJECT TERMS tornadoes, boundary layer, supercell, shear, static stability	**15. NUMBER OF PAGES** 47
	16. PRICE CODE

17. SECURITY CLASSIFICATION OF REPORT	**18. SECURITY CLASSIFICATION OF THIS PAGE**	**19. SECURITY CLASSIFICATION OF ABSTRACT**	**20. LIMITATION OF ABSTRACT**
Unclassified	Unclassified	Unclassified	UU

NSN 7540-01-280-5500

Standard Form 298 (Rev. 2-89)
Prescribed by ANSI Std. 239-18

THIS PAGE INTENTIONALLY LEFT BLANK

Approved for public release. Distribution is unlimited.

THE INFLUENCE OF BOUNDARY-LAYER SHEAR AND STATIC STABILITY ON LOW-LEVEL VERTICAL ACCELERATIONS IN A SUPERCELL

Sean P. Caulfield
Lieutenant Commander, United States Navy
BS, Western Carolina University, 2007

Submitted in partial fulfillment of the
requirements for the degree of

MASTER OF SCIENCE IN METEOROLOGY AND PHYSICAL OCEANOGRAPHY

from the

NAVAL POSTGRADUATE SCHOOL
December 2018

Approved by: John M. Peters
Advisor

Qing Wang
Second Reader

Wendell A. Nuss
Chair, Department of Meteorology

THIS PAGE INTENTIONALLY LEFT BLANK

ABSTRACT

It is well documented that tornadoes are formed from a special breed of rotating thunderstorms called supercells, and that tornadogenesis is a result of several factors, one of which is the vertical stretching of low-level vorticity. Not as well understood are the factors that contribute to vertical acceleration of low-level vorticity in the updraft region of a supercell to support tornadogenesis. This paper examined the influence of combining both low-level shear and low-level static stability on low-level vertical accelerations using idealized simulation from Cloud Model 1 (CM1). A matrix of simulations varied the low-level shear and the low-level convective inhibition (CIN) in order to parse out the dynamic response of these parameters on the low-level forcing. When shear was added to simulations, there was a consistent positive response to the low-level dynamic forcing; when low-level CIN was increased, there was a consistent negative response to the low-level buoyant forcing. Despite the chaotic nature of a supercell environment, a balance can be achieved in the lower atmosphere where the low-level CIN can counteract the low-level shear and inhibit the vertical stretching of vorticity. Since this phenomenon is associated with tornadogenesis, a correlation can be made between the ratio of low-level static stability to low-level shear and its effect on tornado formation.

THIS PAGE INTENTIONALLY LEFT BLANK

TABLE OF CONTENTS

THIS PAGE INTENTIONALLY LEFT BLANK

LIST OF FIGURES

THIS PAGE INTENTIONALLY LEFT BLANK

LIST OF TABLES

THIS PAGE INTENTIONALLY LEFT BLANK

ACKNOWLEDGMENTS

Many thanks for the help and support of my advisor, Dr. John Peters, my second reader, Dr. Qing Wang, and the staff of the Oceanography and Meteorology departments, whose guidance made this document possible.

THIS PAGE INTENTIONALLY LEFT BLANK

I. INTRODUCTION

Tornados are the subject of countless scientific papers, books, and even Hollywood movies due to their societal and economic impacts. Nearly all damaging tornadoes are produced by a special breed of rotating thunderstorms called supercells (Gallus et al. 2008). Around 800–1,400 tornados are reported each year in the U.S. (Ashley 2007) and have caused around 1,000 deaths over the past decade. In 2011 alone, tornadoes cost $28 billion in damages (Simmons et al. 2013). Starting with John Park Finley's tornado research of the 1880s to the most recent research of Nowotarski et al. (2011), Naylor and Gilmore (2014) and Coffer and Parker (2015, 2017), scientists have tried to better understand the dynamics of tornadic thunderstorms with the end goal of improving their predictability. However, despite the multitude of studies conducted to better understand supercells and tornadoes, accurately predicting whether a supercell will produce a tornado remains challenging (Anderson-Frey et al. 2016, Coffer and Parker 2017).

The formation of supercell thunderstorms requires that moderate-to-strong vertical wind shear be present in an environment with convective available potential energy (CAPE) (Weisman and Klemp 1982). Vertical wind shear is the change in wind speed and/or wind direction with height. Deep layer shear generally refers to the shear between the surface and 6–8 km, whereas low-level shear generally refers to the shear between the surface and 1–3km. Generally, stronger deep layer shear gives rise to supercells, whereas weaker deep-layer shear yields modes of convection that are less organized on the scale of individual storms. Rotation in supercells originates from the vertical tilting of low-to-mid level horizontal vorticity associated with low-level shear. Low-level shear can therefore increase the vorticity of an updraft, and the associated rotationally-driven dynamic low pressure in the lower updraft (Weisman and Rotunno 2000, Davies-Jones 2003). This leads to stronger upward accelerations within and above the boundary layer, which increases the intensity of the storm's low-level updraft (Coffer and Parker 2015). Low-level updraft intensity is in turn connected to the stretching of low-level vertical vorticity, which facilitates tornadogenesis. Environments that have sufficient CAPE and low-level shear can lead to supercell development and set up a regime that supports tornadogenesis.

Conversely, convective inhibition (CIN) has the opposite effect, in that it suppresses upward vertical motion of an air parcel, and subdues tornadogenesis as shown by Nowotarski et al. (2011).

As previously mentioned, low-level shear is critical to supercell development and studies have shown that low-level shear velocities exceeding around 10 m s^{-1} are conducive to strong thunderstorms (Thompson 1998, Thompson 2003, Rasmussen and Blanchard 1998). One of the most prominent sources of low-level shear in the central United States is the Low-level Jet (LLJ). The LLJ is a wind maximum in the lower levels (e.g., 500 m to 1 km) of the atmosphere and has typical velocities around 20 m s^{-1} (Shapiro and Federovich 2009). Since the LLJ typically occurs in conjunction with relatively light near-surface flow because of the nocturnally stabilized boundary layer, sufficient low-level shear is often present below the LLJ for tornadogenesis. The LLJ is diurnally modulated and reaches a maximum during the night and a minimum during the day (e.g., Du and Rotunno 2014). Because the LLJ is synonymous with increased low-level shear, this feature is of critical importance to tornadogenesis as the low-level shear magnitude positively correlates to the strength and persistence of tornadic supercells (Coffer and Parker 2015).

Near surface thermal effects are also critical to supercell development because they have an important impact on the CAPE and CIN of boundary layer air parcels. Throughout the day, the sun is consistently heating the earth with shortwave radiation. The radiation heats up the boundary layer and can initiate convective storms as parcels become warmer, and more buoyant than their surroundings. After the sun sets, the ground cools due to a reduction in incoming shortwave radiation, and both static stability and CIN increase in the boundary layer. Storms are often able to sustain themselves overnight despite this increase in CIN because a layer of air with high CAPE and low CIN from above the surface feeds the storms (these types of storms are called “elevated,” Corfidi et al. 2008). Since it is generally understood that the upward acceleration of near-surface air below an updraft is necessary for tornadogenesis, and this near-surface upward acceleration is inhibited when storms become elevated, elevated supercells should have lower probabilities of producing tornadoes. Despite this, although commonly observed, the prevalence of nocturnal tornadoes is poorly understood. One of the findings from Nowotarski et al. (2011) is that

the presence of a stable boundary layer inhibits the development of near-surface vorticity in supercells. The magnitude and location of the cold pool relative to the updraft of the supercell are important factors to consider when predicting the strength of a supercell thunderstorm and the magnitude (if present) of low-level rotation (Nowotarski et al. 2011).

A more difficult question to answer is how a supercell thunderstorm responds to a combination of the LLJ and low-level CIN, which increase in magnitude with time after dark. Strong low-level accelerations are critical for the vertical stretching of vorticity and the subsequent spin-up of tornadoes (Markowski and Richardson 2014, Coffer and Parker 2017). Coffer and Parker (2015) demonstrated that an increase in the LLJ corresponded to stronger dynamic accelerations in the lowest levels of the storm, and the enhanced LLJ consequently increased the likelihood of tornadogenesis. However, Coffer and Parker (2015) kept the low-level stability thermodynamic parameters constant in their experiments. Nowartarski et al. (2011) studied how varying the magnitude of low-level static stability would affect the ability for a supercell to produce rotation at the lowest levels and found that increasing low-level static stability generally decreased the intensity of buoyant accelerations in the lower updraft. However, Nowartarski et al. (2011) used a constant wind profile in their experiments. To date, there are not any studies that vary both low-level static stability and low-level shear, and assess the combined influence of these factors on low-level vertical accelerations. Due to the transitional characteristic of the lower atmosphere after sunset (i.e., low-level static stability and LLJ magnitude increases), an effort of this study is to determine what characteristics of the nocturnal environment are still capable of producing tornadic supercells.

The goal of this study is to understand how the combined effect of increasing low-level shear and low-level CIN with time influence a supercell's low-level accelerations and potential for tornadogenesis. This is accomplished by running a series of numerical simulations of supercells, wherein the temperature at the surface and the strength of the wind shear below 1km are varied among runs. The hypothesis is that increasing the near-surface stability and CIN among simulations reduces storms' low-level buoyant accelerations, and increasing the low-level shear in addition to the CIN increases storms' low-level dynamic accelerations. As a consequence, there are a range of environments

where the positive influence of increasing low-level shear on tornadogenesis offsets the deleterious effects of increasing CIN on tornadogenesis. The organization of this thesis is as follows: Chapter II discusses the methods to address the objectives of this thesis. Chapter III presents the results of the model simulations. Discussion and conclusions are given in Chapter IV.

II. METHODS

Cloud Model 1 version 18 (CM1v18) (CM1, Bryan and Fritsch 2002) was used for the numerical simulations in this study. CM1 is a non-hydrostatic model with an acoustic time stepping scheme. The simulations were configured with free-slip top and bottom boundary conditions and open-radiative lateral boundary conditions (LBCs) (e.g., Klemp and Durran 1983). Microphysics were represented by the Morrison et al. (2005) double moment scheme with graupel and snow as the prognostic ice hydrometeor species. The simulations did not contain any radiation physics or surface fluxes. Convection was initiated by including a 5 km wide and 1 km deep warm bubble in the initial conditions, which was located at the center of the domain and centered at 1500 m above ground level. This warm bubble has a temperature that is 1.5 K higher than its surroundings. Table (1) highlights all of the CM1 parameters used in our simulations. Model simulations used two setups of grid/time step resolutions in a 50 km × 50 km box: a coarser resolution of 1 km horizontal and 250 m vertical grid spacing, and 3.75 s time step, and a finer resolution of 250 m horizontal and 100 m vertical grid spacing, and 1.25 s time step. The coarser resolution runs were used as initial benchmarks for our modeling setup, and only the results from the 250 m resolution runs are included hereafter. The higher resolution simulations were run with the Naval Postgraduate School Hamming supercomputing cluster. The modeled storms' horizontal velocity was subtracted in order to keep the frame of reference centered and storm-relative. The domain translated North at 8.5 m s^{-1} and East at 4.5 m s^{-1}, which is synonymous in this instance to subtracting the mean wind due to the free slip boundary layer.

In most simulations, the initial supercell split into a right-mover and left-mover, and the domain followed the characteristically stronger right-mover. Different domain sizes and resolutions were tested throughout the experiment and the results were unaffected by these changes. Hence, the focus in the results and discussion will remain with the higher resolution simulations. To initialize the model run for the control run, CM1 ingested a sounding and hodograph as indicated in Figures 1 and 2. The details of this initial model profile are discussed later in this section.

Table 1. Overview of the CM1 model configuration

Attribute	*Value/setting*	*Notes*
Fully compressible	yes	
Horizontal grid spacing	250 m	
Vertical grid spacing	100 m	
Vertical coordinate	height (m)	
Number of x and y points	400 x 400	
Vertical points	180	
Top/bottom LBCs	free-slip	
North/south LBCs	open-radiative	Durran and Klemp (1983)
East/west LBCs	open-radiative	Durran and Klemp (1983)
Convection initiation	warm bubble at domain center, horizontal radius: 5 km, vertical radius: 1.4 km, θ perturbation: 3 K	
Microphysics	Morrison	Morrison et al. (2005)
Diffusion	6th order	
Subgrid turbulence	TKE	
Rayleigh dampening	yes	
Dissipative heating	yes	
2nd and 6th order diff. coef.	75 - .04	
Longwave radiation	none	
Shortwave radiation	none	
Surface layer	none	
Boundary layer physics	none	
Cumulus parameterization	none	

The strategy for this experiment was to vary the low-level stability and low-level wind shear among simulations, and to assess both the separate and the combined impact of these parameters on low-level vertical accelerations (Table 2). For the simulations, a modified Weisman and Klemp (1982, hereafter WK82) analytic sounding was used to initialize the model. The WK82 sounding has been used in previous studies (e.g., Nowotarski 2011) and is similar to the warm season environments in the central United

States that typically foster supercell thunderstorms. The boundary-layer mixing ratio in this sounding was set to 16 g kg^{-1}, which yielded a 0–1 km mean CAPE of ~ 2700 J kg^{-1}. The control group featured a quarter-circle shaped hodograph (Rotunno and Klemp 1982, hereafter RK82; this profile is referred to as "S1"), which is also consistent with tornadic supercell environments (e.g., Parker 2014). This profile featured clockwise turning shear in the lowest 1 km, and shear with no directional change above 1 km. This configuration is slightly different than that of RK82, wherein clockwise turning shear extended from the surface to 2 km. However, the wind profile configuration here is more consistent with observed tornado environments where shear curvature is typically confined to the lowest 1 km. The deep-layer shear magnitude of 31 m s^{-1} in this sounding is consistent with past observational studies of the environments of tornadic supercells (e.g., Markowski et al. 2003, Parker 2014). The 0–1 km shear in the S1 profile was 10.4 m s^{-1}, and the 0–1 km and 0–3 km storm-relative helicity (SRH) magnitudes were 174 and 255 J kg^{-1}, respectively. In the experiments where the shear magnitude was increased (henceforth, this profile is referred to as "S2"), the length of the hodograph in the v direction was doubled below 1 km, and the hodograph also followed a sinusoidal shape in the 1–2 km layer. Both hodographs are plotted for reference in Figure (2). S2 yielded a new 0–1 km shear magnitude of 19.5 m s^{-1} and 0–1 km and 0–3 km storm-relative helicity (SRH) magnitudes were 341 and 390 J kg^{-1}, respectively.

Consistent with the experimental methodology of Nowotarski et al. (2011), low-level stability was modulated in each run by progressively reducing the surface temperature (θ_0), and prescribing a linear increase in θ_0 between the value at the surface and that in the control profile at 500 m. Starting with a θ_0 of 300K, static stability was increased by decreasing θ_0 to discriminate values of 297K, 295K, and 293K as indicated in Figure (3). Surface-based CAPE (CIN) values for these static stability variations were 2620 J kg^{-1} (-20 J kg^{-1}), 1925 J kg^{-1} (-70 J kg^{-1}), 1502 J kg^{-1} (-97 J kg^{-1}), and 1136 J kg^{-1} (-123 J kg^{-1}), respectively. CAPE and CIN above 500 m were held constant among the profiles. The surface cooling was given ranges that could realistically simulate the potential surface cooling that occurs during the nighttime transition of the boundary layer from latent heat release and radiative cooling.

Table 2. CM1 model design and configurations

		Low-level Shear (0-3 km)	
		S1=10m/s	S2=20m/s
Surface Temperature (K)	300K	300KS1 (Control)	300KS2
	297K	297KS1	297KS2
	295K	295KS1	295KS2
	293K	293KS1	293KS2

This table is an overview of the simulations that were run where 300KS1 indicates a shear value of 10 m s^{-1} and a surface temperature of 300K, 295KS2 indicates a shear value of 20 m s^{-1} and a surface temperature of 295K, etc.

Figure 1. Analytic initial conditions for the control

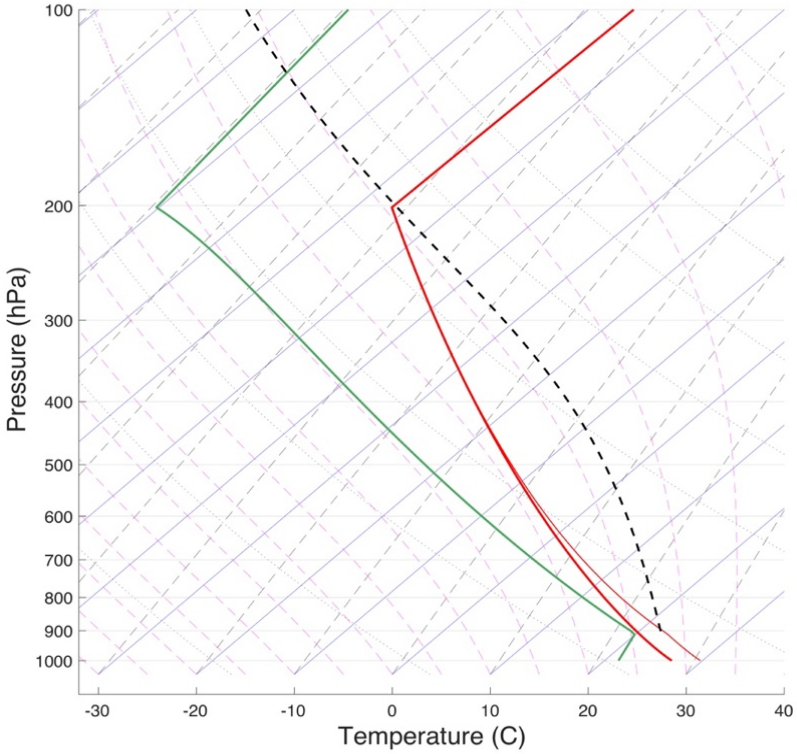

Skew-T log-P diagram of the analytic sounding used to initialize CM1. Thick red line: temperature, thin red line: virtual temperature, green line: dew point temperature, and dashed black line: the temperature for a lifted air parcel with the average properties of the lowest 1 km.

Figure 2. Hodographs showing wind shear setup for S1 and S2 simulations

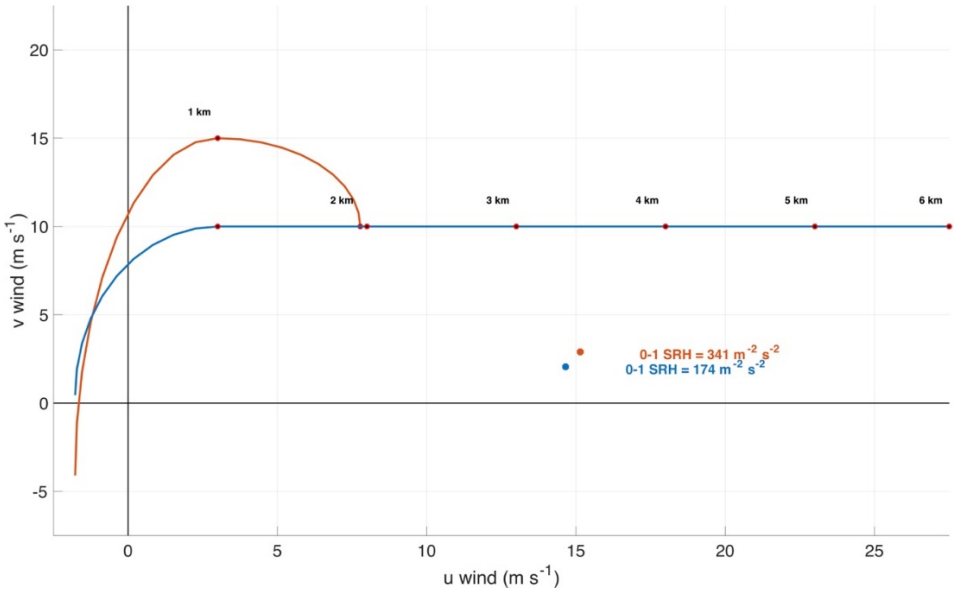

Hodograph showing the clockwise turning of wind vectors in the lowest 1km of the atmosphere. U-wind velocity (m s^{-1}) is on the x-axis and V-wind velocity (m s^{-1}) is on the y-axis. Also indicated are the 0–1km Storm relative helicity (SRH) (m^2 s^{-2}). The blue line represents the S1 wind profile and the red line represents the S2 wind profile. Storm motion vectors for S1 and S2 are blue and red dots, respectively, and are estimated using the method of Bunkers et al. (2000).

Figure 3. Low level stability profiles of the simulated environment for control and all θ_0 simulations

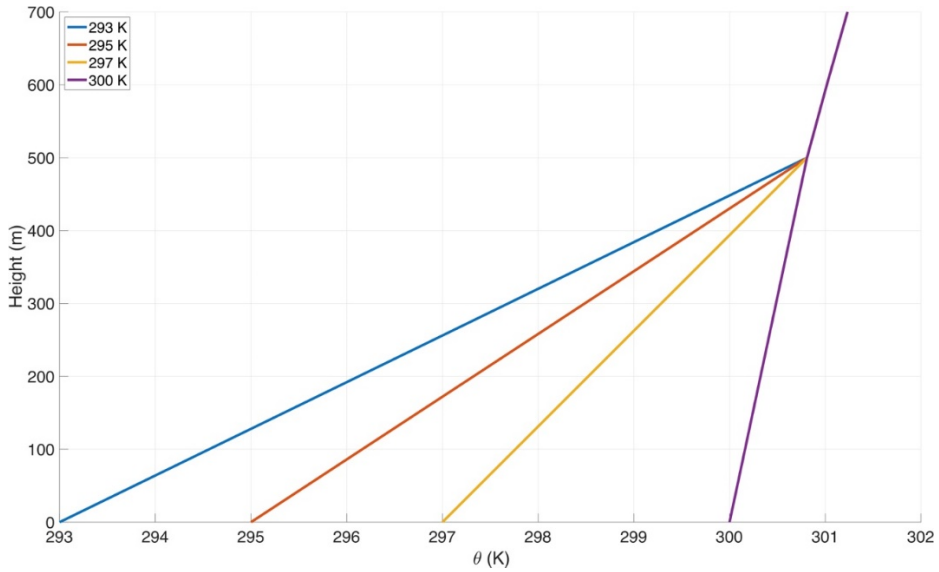

Graph indicating potential temperature (K) as a function of height (m) used in all simulations. The legend gives the surface potential temperature for each profile.

A total of eight simulations were run covering the two wind profiles and the four thermodynamic profiles. Tornadoes typically have spatial scales of 50–500m, which requires grid spacing <50m for the proper resolution of a tornadic circulation (there were insufficient computational resources to run the model at this resolution). The 250m grid spacing of the simulations was therefore insufficient to properly resolve tornadoes. Despite this, Nowatarski et al. (2011) showed that surface vorticity associated with tornado-like circulations can be used to evaluate the tornado production potential of simulated storms. Temporal variations of the surface and 1 km vorticity were therefore created to compare the results from different model simulations and assess the potential for tornadogenesis. Real world tornadoes can have low level vorticity on the scale of 0.1–1 s^{-1}, so by producing the time series plots one could assess when or if vorticity magnitudes that were sufficiently high to correspond to tornadic circulations were produced.

Further data analysis of the results was made in order to assess influences of the low-level stability and low-level vertical wind shear on the supercells' low-level accelerations. The low-level accelerations and forcing can be assessed by first starting with the Lagrangean Boussinesq vertical vorticity equation which can be written as

$$\frac{d\zeta}{dt} = \underbrace{\zeta \frac{\partial w}{\partial z}}_{Stretching} \underbrace{- \nabla w \cdot \nabla \times \boldsymbol{V_h}}_{Tilting},$$

where ζ is the vertical vorticity and $\boldsymbol{V_h}$ is the horizontal wind vector. Since $\frac{\partial w}{\partial z}$ in the stretching term is well correlated with $\frac{dw}{dt}$ for upward moving air parcels, regions of upward accelerations in the presence of background vertical vorticity will cause the magnitude of vertical vorticity to increase with time. This is because air columns horizontally contract as they are vertically stretched, and because conservation of angular momentum dictates that a spinning air column that horizontally contracts with time must spin faster (much like an ice skater who brings their arms in while spinning). Environmental properties such as stability and shear consequently directly influence tornadogenesis via the influence of these attributes on vertical accelerations.

To understand how stability and shear influence accelerations, we write the total acceleration of an upward moving air parcel for an anelastic atmosphere as

$$\frac{dw}{dt} = \underbrace{B - \frac{1}{\rho_0}\frac{\partial p'_b}{\partial z}}_{\substack{Buoyant \\ Accelerations}} \quad \underbrace{- \frac{1}{\rho_0}\frac{\partial p'_d}{\partial z}}_{\substack{Dynamic \\ Accelerations}} , \tag{1}$$

where the model's initial state variables are denoted by subscript 0 and deviations from this initial state are denoted by primes, $B \equiv -g\frac{\rho'}{\rho_0} - r_i$ is the buoyancy defined relative to the model's initial state (where r_i is the mixing ratio of the ith hydrometeor species; e.g., rain, snow, graupel), $-\frac{1}{\rho_0}\frac{\partial p'_b}{\partial z}$ is the vertical pressure gradient force from buoyancy pressure, $-\frac{1}{\rho_0}\frac{\partial p'_d}{\partial z}$ is the vertical pressure gradient force from dynamic pressure (hereafter "dynamic forcing"), and net buoyant accelerations are described by $B - \frac{1}{\rho_0}\frac{\partial p'_b}{\partial z}$ (hereafter "buoyant forcing"; e.g., Parker and Johnson 2004). The definitions for p'_d and p'_b are

$$\nabla^2 p'_b = \frac{\partial(\rho_0 B)}{\partial z} \tag{2}$$

$$\nabla^2 p'_d = -\nabla \cdot [\rho_0 (\boldsymbol{V} \cdot \nabla)\boldsymbol{V}] \, . \tag{3}$$

Since buoyant forcing is strictly a function of density variations, it is exclusively determined by an updraft's thermodynamic properties. Regions that are locally warmer (cooler) than their surroundings typically experience upward (downward) buoyant forcing. Boundary-layer air with low (high) CIN that is ingested into an updraft should become locally warmer (cooler) than its surroundings and therefore experience enhanced (dampened) upward accelerations from buoyant forcing. Thus, the relative magnitudes of buoyant forcing in the lower updraft can be compared among simulations to assess the influence of modifications to the low-level stability on the updraft's vertical accelerations, since storms in the less (more) stable low-level environments should have larger (smaller) low-level buoyant forcing.

On the other hand, dynamic forcing is primarily a function of spatial gradients in air velocity, and the spatial distribution of dynamic forcing is often dominated by upward accelerations beneath a supercell's rotationally-driven low-pressure maxima (Rotunno and Klemp 1982). We may therefore compare the distributions of dynamic forcing in the low-level updraft among simulations to assess the influence of the low-level shear on updraft accelerations. Storms in the environments with the strongest (weakest) low-level shear

should rotate the fastest (slowest), have the most (least) intense rotationally-driven low-pressure maxima, and have the largest (smallest) low-level dynamic forcing. Particular emphasis was given to the lowest 1 km of the atmosphere, because this is the layer where the influence of low-level accelerations on tornadogenesis is most critical (e.g., Markowski and Richardson 2014, Coffer and Parker 2015, 2017).

III. RESULTS

An initial examination of simulated radar reflectivity plots from the control (300KS1) run shows a supercell thunderstorm with a clear hook echo and updraft regions (Figure 4A). All simulations within the experiment produced a supercell and were verified by the radar reflectivity for the key supercell features mentioned above. All further analysis concentrates on the right-moving, dominant supercell in the model domains. Composite simulated reflectivity plots are shown here (Figure 4), rather than snapshots from individual times, because they are most representative of the supercell's structure through a longer period in the simulation. To create the composite figures, the right-moving domain supercell was first objectively tracked by averaging the vertical velocity in the 0–4 km layer, averaging the vertical vorticity in the 0–4 km layer, ignoring regions with negative 0–4 km average vertical vorticity, and selecting the largest remaining continuous area of 0–4 km averaged vertical velocity with $w > 3$ m s^{-1}. The center point of this region was defined by a vertical velocity weighted average location. The Figures 4A-H were then created by averaging the, updraft centered, CM1 reflectivity output from 1km from minute 75 to minute 150 of the simulations. The results from the tracking procedure were then visually analyzed to ensure that the procedure produced a track that corresponded to the dominant right-moving supercell. The black outline on Figures 4A-H indicates the average updraft region and was created by averaging the 1–4km vertical velocities from that were > 6 m s^{-1}.

An examination of the composites revealed a few expected results. In the cooler θ_0 runs (295K and 293K) (Figures 4E-4H), the cold pools were much weaker and less expansive compared to the 300K (Figures 4A and 4B) runs. This result is most dramatic when comparing the 300K runs to the 293K runs and can be identified by the spatial extent of the surface temperature perturbation (θ‘), the light blue lines on Figure 4. This was expected because as the cool air falls through the downdraft and reaches the surface, θ‘ is not as apparent due to the lack of contrast between the initial surface theta and the rain-cooled downdraft air. The cold pool was slightly weaker in the vicinity of the updraft in

the S2 runs than in the S1 runs, which is potentially a result of an increase in the northward advection of hydrometeors away from the updraft due to the increased shear.

Figure 4. Composite reflectivity plots

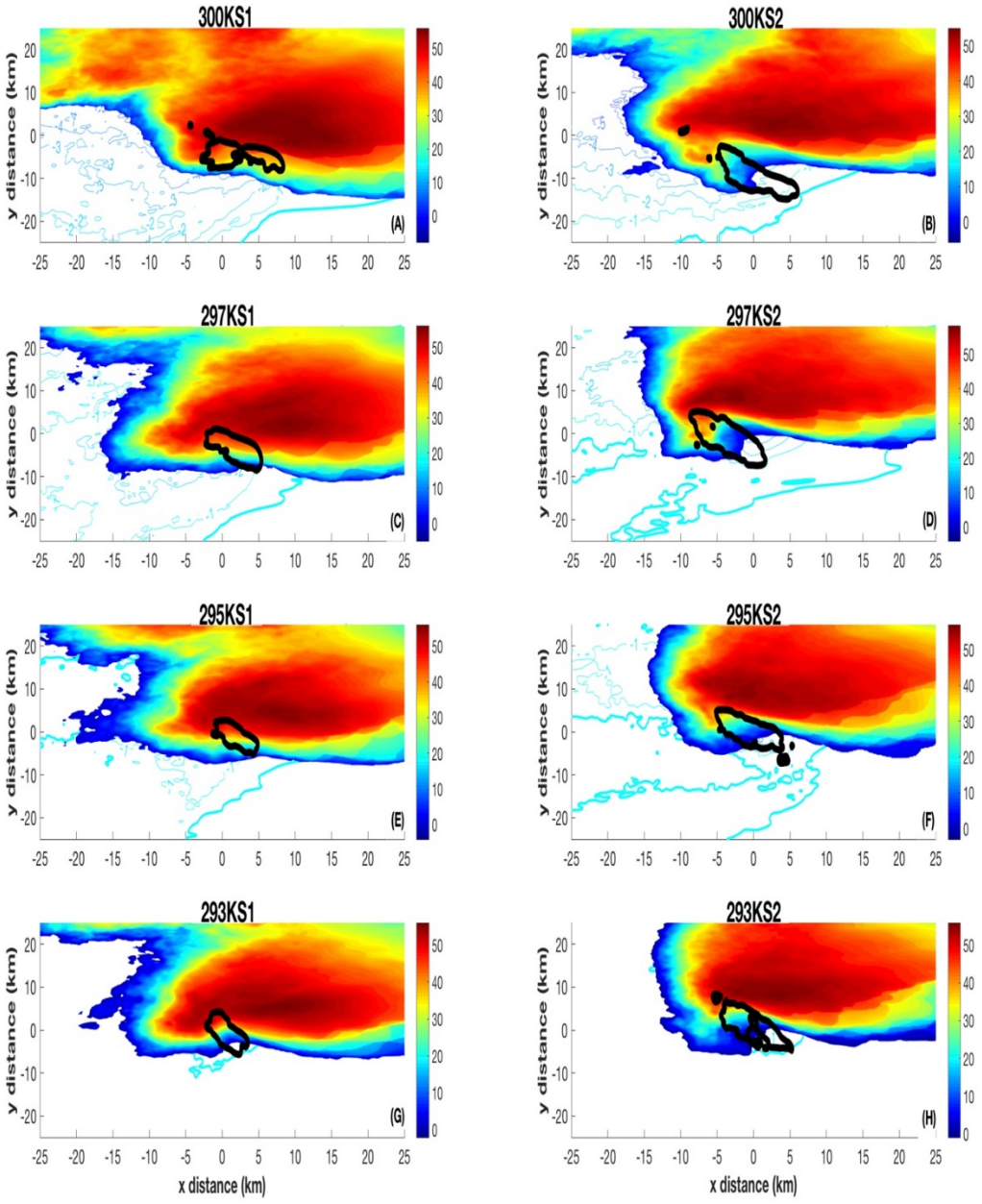

In this figure, the simulated reflectivity in dBZ (the shaded region) of the supercells is plotted with θ‘ (K) with the thicker cyan lines indicating the 0K θ‘ and the lighter cyan lines are the subsequent single degree θ‘. The composite plots are the averaged 5 minute reflectivity output at 1km from minutes 75–150 of the simulations. The updraft region of the supercells is highlighted by the black outline on the plots.

The time series of surface vorticity (Figure 5) and 1 km vorticity (Figure 6) indicated there were several instances within all the simulations where the vorticity fluctuated substantially over time, with distinct temporal peaks and troughs. This temporal variability is a result of the chaotic nature of supercells. The periodic strengthening and weakening during the lifetime of a supercell has been shown in previous research (Adlerman and Droegemeier 2005) and supercells' behavior are often extremely sensitive to subtle variations in internal and background environmental characteristics (Coffer et al. 2017). Henceforth, the control (300KS1) and the shear modulated control (300KS2) runs are plotted on all figures for easier comparison between the simulations. 300KS1 is always a solid blue line and 300KS2 is always a solid red line.

Consistent with Parker et al. (2015), by increasing the low-level shear in the 300K profile, there was a dramatic response in the maximum 1 km vertical vorticity in the 300KS2 run, as shown by the doubling of the vorticity towards the end of the simulation (Figure 5). This result is less obvious in the θ_0 simulations, indicating a connection between the magnitude of vorticity and low-level stability. Time series plots of maximum surface vorticity showed similar trends (Figure 6). The peaks in the vorticity time series indicate phases in the supercells' lives when tornadogenesis was most likely.

Figure 5. Time evolution of maximum 1-km vorticity from simulations with surface potential temperature of 297K (A), 295K (B), and 293K (C).

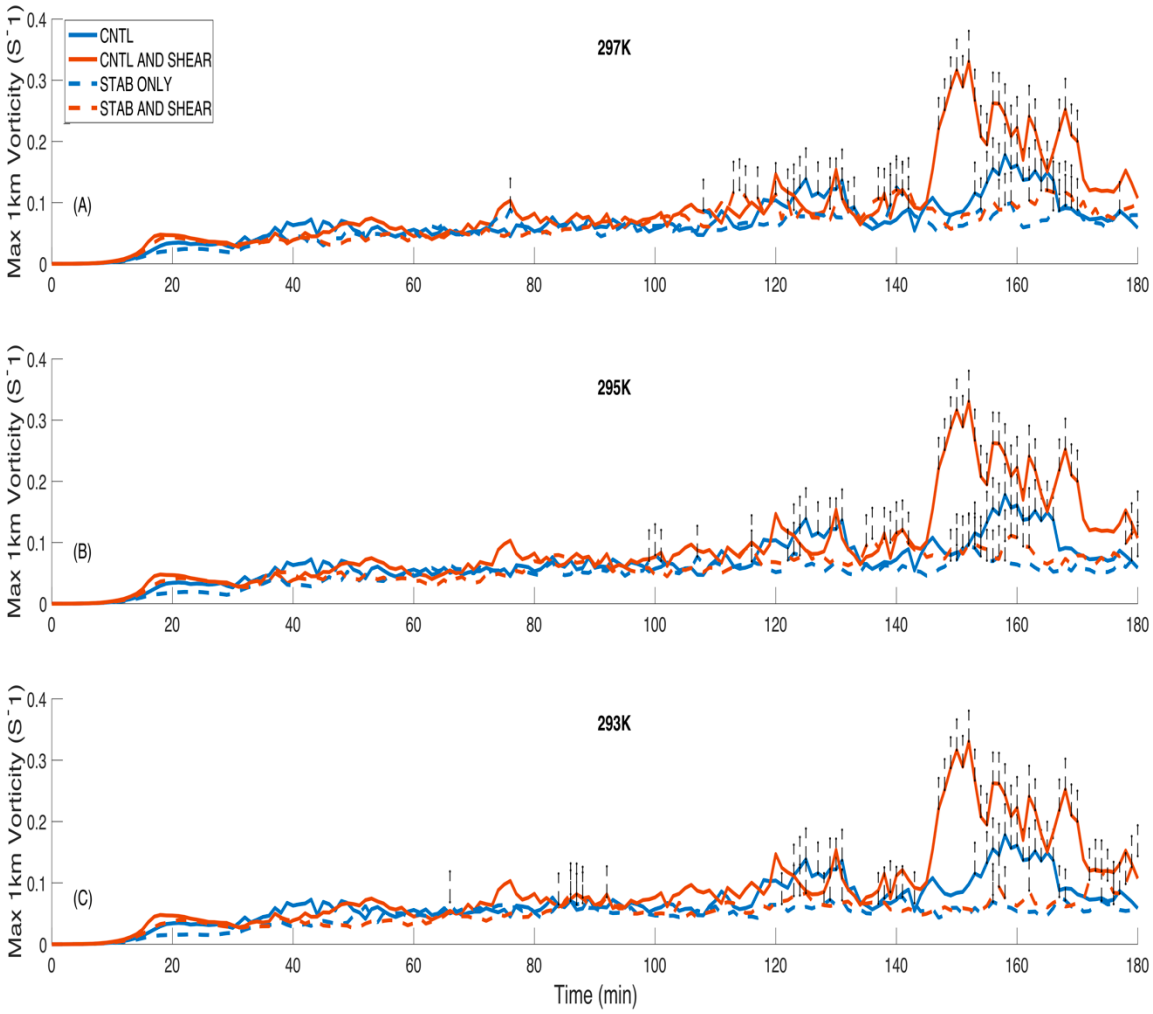

This figure shows the time series of maximum 1-km vorticity (s^{-1}) from 297K, 295K, and 293K simulations. The red lines correspond to the S2 runs and the blue dashed lines correspond to the θ_0 runs. The red dashed lines are the S2θ_0 runs. The black dashed lines indicate the highest 20 surface vorticity values in each run. In accordance with the legend, CNTL is the 300KS1 run, CNTL and shear is the 300KS2 run. Both runs are included on each plot for easier comparison.

Figure 6. Time evolution of maximum surface vorticity for simulations 297K (A), 295K (B), and 293K (B).

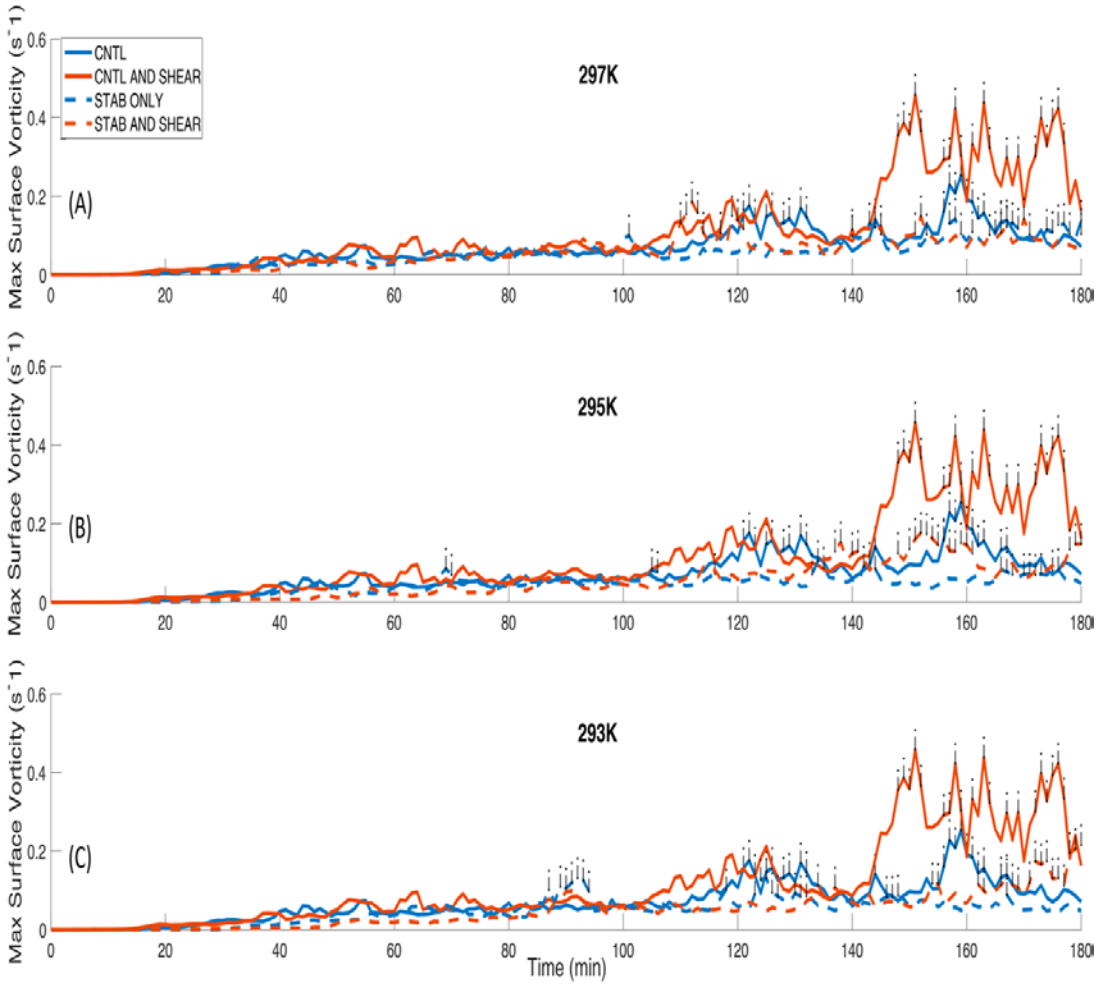

This figure shows the time series of maximum surface vorticity (s^{-1}) for 297K, 295K, and 293K simulations. The red lines correspond to the S2 runs and the blue dashed lines correspond to the θ_0 runs. The red dashed lines are the S2θ_0 runs. The black dashed lines indicate the highest 20 surface vorticity values in each run. In accordance with the legend, CNTL is the 300KS1 run, CNTL and SHEAR is the 300KS2 run. Both runs are included on each plot for easier comparison.

Because of the considerable variability in the vorticity, the 20 largest instantaneous surface and 1 km vertical vorticity values were selected from each simulation for further analysis. The black lines on Figures 5 and 6 indicate the highest 20 values that were selected. These 20 highest values were compared between runs, and were considered to reflect an increased likelihood of tornadogenesis in a given storm. To determine whether

differences in these 20 highest values were statistically significant between simulations, the "bootstrap" statistical method was used (Efron 1978). This technique relies on random sampling with replacement which was done by randomly selecting 20 values within the original 20, with the potential for repeating values, in order to create new samples. The average of each new sample was then taken. This process was repeated 1000 times, and the 95th and 5th percentile averages were used to generate the blue and red boxes in Figures 7A-C. The right (left) side of the box gives the statistical average of the highest (lowest) maximum 1km vorticity of the 1000 resampled data sets and the top (bottom) of the box gives the statistical average of the highest (lowest) maximum surface vorticity of the 1000 resampled data sets. If the edges of two boxes do not overlap (overlap) in the x or y direction, the differences in the averages of the 20 maximum vorticity values between two runs are (are not) statistically significant.

In the 295K (Figure 7B) and 293K (Figure 7C) runs, a few trends are evident. As expected, the 300KS2 run, with larger low-level shear than that 300KS1, produced larger maximum surface and 1 km vorticity magnitudes than the 300KS1. Also, the 297KS1, 295KS1, and 293KS1 runs, with progressively larger near-surface CIN, produced progressively smaller surface and 1 km vorticity magnitudes. Both the 293KS2 (Figure 7B) and 295KS2 (Figure 7C) runs, with both larger stability and shear than the control, showed larger surface vorticity and 1km vorticity than the 293KS1 and 295KS1 runs. In fact, the surface vorticity, and to a lesser extent the 1 km vorticity, of both the 293KS1 and 295KS1 runs shifted in line with the control. All of the findings indicated above were statistically significant as identified by the confidence boxes.

Compared to the 295K and 293K runs, trends for the 297K run (Figure 7A) were not as pronounced. The modest near-surface stability increase in the 297K runs had a similar effect as the 295K (Figure 7B) and 293K (Figure 7C) runs in that it decreased both surface vorticity and 1km vorticity, however, when shear was added to the 297KS1 run, only the max 1km vorticity showed significant response. The lack of response in the surface vorticity is probably because of the small difference in the thermodynamic profile compared to the controls.

Figure 7. 297K (A), 295K (B), and 293K (C) vorticity scatterplots

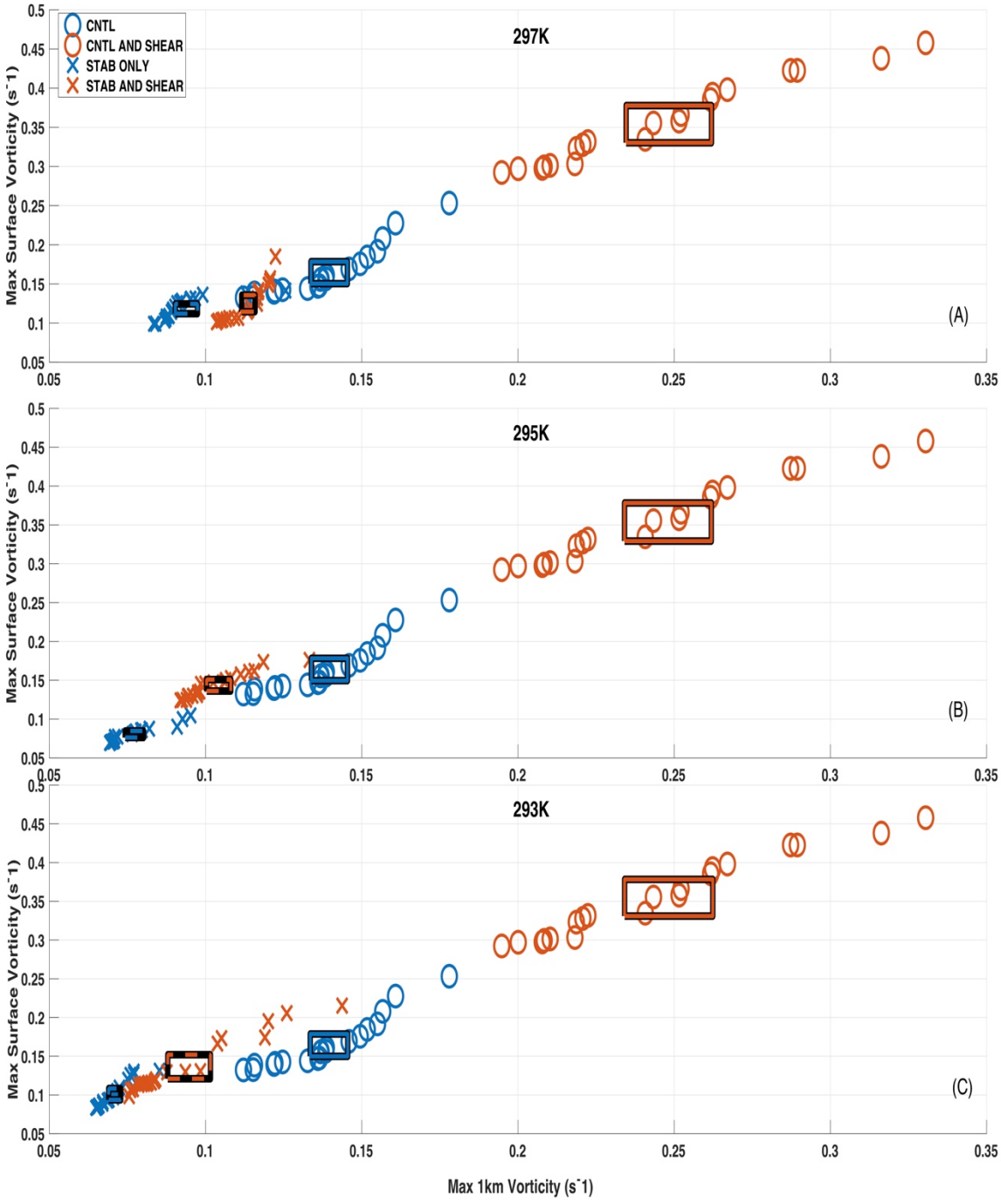

Illustrated here is a scatterplot of the highest 20 values of1km vorticity vs surface vorticity (s^{-1}). The top and right sides of the boxes indicate the 95th percentile of the surface vorticity and 1km vorticity, respectively, and the bottom. and left sides of box indicate the 5th percentile of the surface vorticity and 1-km vorticity, respectively.

To connect the low-level stability and shear differences among runs to the vorticity differences described above, the vertical profiles of buoyant and dynamic accelerations in the lower updraft were examined and time averaged from 100 min to 180 min in each simulation. Figures 8A-C show the profiles of updraft forcing for the all three θ_0 simulations, 297K, 295K, and 295K, respectively. The forcing plots were broken up into the buoyant and dynamic forcing components and then added together to get the net forcing. The 300K runs are also shown on the same plots for comparison. In the 300KS1 control run, the low-level forcing is driven by a combination of strong upward buoyant and dynamic forcing below 1 km. When shear was added to the control run to get 300KS2, there was a dramatic increase in the low-level dynamic forcing, and little change in buoyant forcing. The net forcing in this case was exclusively due to the addition of shear and therefore, the increase in low-level dynamic forcing. In contrast, the buoyant forcing below 1 km progressively declined relative to the 300K runs as shown by the dashed lines in Figure 8A (297K), Figure 8B (295K), and Figure 8C (293K) runs, indicating that the effect of the low-level stability in these runs on updraft forcing was reflected in the buoyant forcing distribution.

The net forcing plots also indicate that by adding low-level shear to the 297KS1, 295KS1, and 293KS1 runs, that as the dynamic forcing increased and the buoyant forcing decreased, the net low-level forcing resembled that of the control near the surface. This is illustrated by the red dashed lines in net forcing column of Figures 8A-C shifting to the right of solid blue line. This is due in part because of the offsetting effects of the stability and shear. In fact, by adding shear, the 295KS2 and 297KS2 runs had higher net forcing than that in the 300KS1 control run throughout the atmosphere. The 293KS2 run is the only run where the net forcing was not as strong as the control. To reiterate, low-level buoyant forcing and dynamic forcing are essential to the spin-up and stretching of low-level vorticity and low-level vorticity is an ingredient of tornadogenesis. The stability and shear induced changes to updraft forcing discussed in this section therefore have a direct impact on the probability of tornadogenesis.

Figure 8. 297K (A), 295K (B), and 293K (C) forcing plots

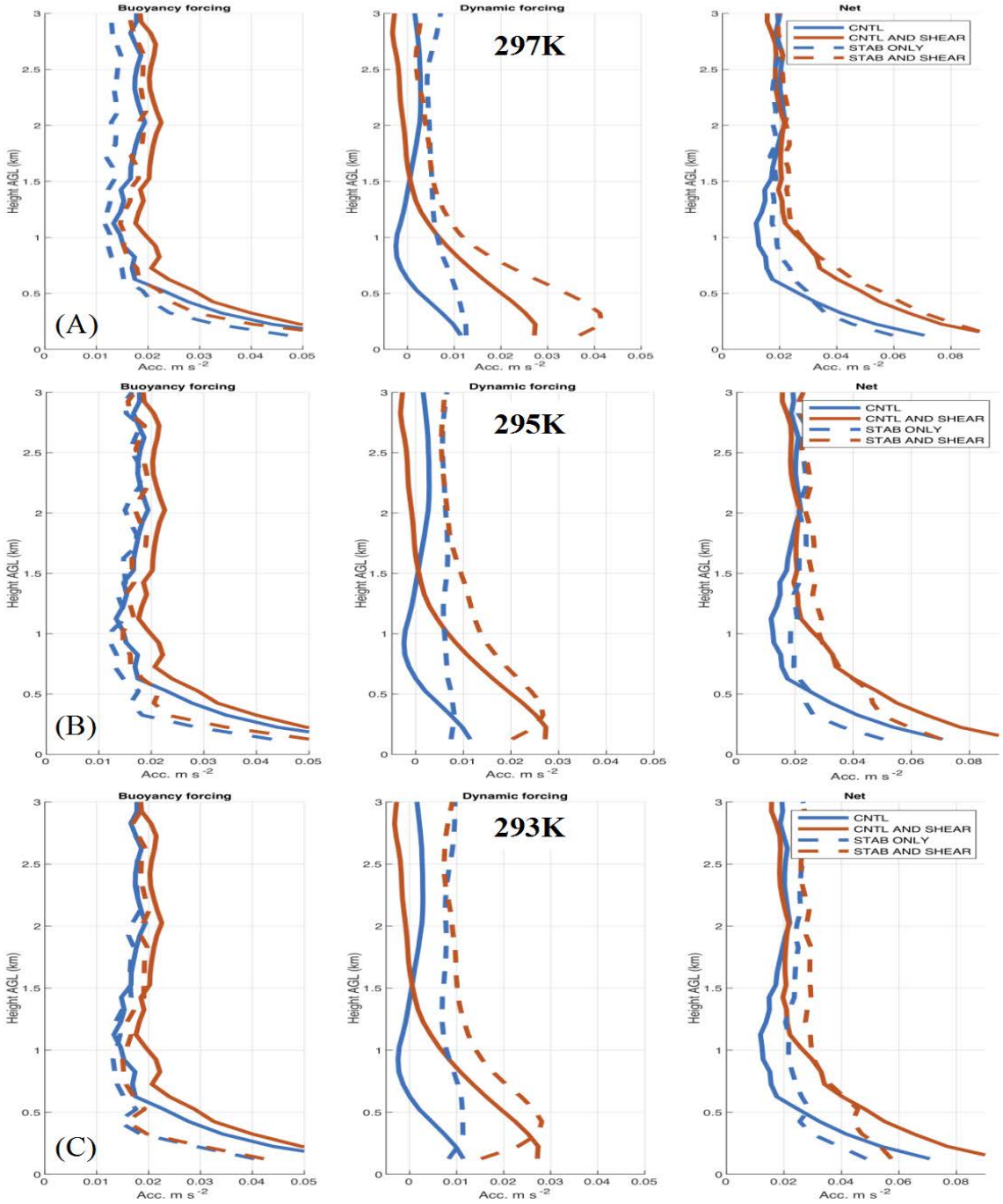

This shows the accelerations (m s^{-2}) on an air parcel at different heights above ground for both the buoyant (left column) dynamic (middle column) and net (right column) forcing mechanisms. The dashed lines are the θ_0 runs. The red lines are the S2 runs. The solid blue line is the 300KS1 run.

THIS PAGE INTENTIONALLY LEFT BLANK

IV. DISCUSSION AND CONCLUSIONS

A. HYPOTHESIS SUPPORT

The following are results from this numerical experiment that helped support my hypothesis. First, it is evident that the dynamic forcing is directly linked to changes in the low-level shear and the buoyant forcing is directly linked to changes in the low-level stability, since increasing the low-level shear while keeping the thermodynamic profile fixed enhanced the low-level dynamic pressure forcing, and increasing the low-level stability while keeping the wind profile constant decreased the low-level buoyant forcing. Second, there is a point in the simulations, and one could assume in the real atmosphere, that dynamic forcing associated with the low-level shear is capable of directly counteracting the decreased buoyant forcing associated with the stability. In this experiment, that tipping point occurred between a θ_0 of 295K and 293K, when the magnitude of 0–1 km vorticity increased by 50 %. Lastly, the low-level buoyant forcing was minimally affected when θ_0 was set to 297K, indicating that marginal low-level stability may have little impact on low-level buoyant forcing.

My hypothesis is supported primarily by the findings in the buoyant and dynamic forcing. The results in Figures 8A-C are consistent with the assumptions that increasing shear can overcome static stability in the lower atmosphere. From the lowest 1km dynamic forcing, it can be seen that by adding shear in the simulations, the dynamic forcing increased (i.e., the red dashed line shifted to the right of the blue dashed line). The decrease in dynamic forcing through the 500 m–1000 m layer was potentially due to the center of the enhancement in the dynamic low pressure having resided near 500 m, which caused an increase in upward forcing below 500 m, but a decrease in upward forcing above 500 m. Along the same lines, the buoyant forcing also performed as expected given the theory behind the accelerating air parcel. When comparing the buoyancy forcing in Figures 8A-C, the two dashed lines “shift” closer to the control as low-level static stability decreases. This corresponds to the inverse relationship between static stability and buoyant forcing.

Furthermore, the scatterplots shed light on the statistical significance and unique difference of each run when comparing the surface and 1km maximum vorticity. Surface vorticity is a key ingredient to tornadogenesis and this experiment illustrated the response of vorticity to low-level stability and low-level shear. Throughout all simulations, brief periods of increased surface vorticity, linked to increased dynamic and buoyant forcing, can increase the probability of tornadogenesis. Likewise, all simulations exhibited lulls or troughs of surface vorticity and correspond to timeframes when tornado formation is less likely.

B. INCONSISTENCIES

Previous research has shown (Coffer et al. 2017) that modeling a supercell thunderstorm can produce a wide variety of results, so it was not surprising that there would be unexpected findings, despite the fact this is was a "controlled" environment and not the real-world. Given that understanding, the following inconsistencies were found with possible explanations ascribed:

1) The time evolution of the max 1km vorticity and surface vorticity do not have an identified trend. There were periods within the θ_0 simulations where the vorticities were higher than the S2 runs, and even higher than the 300KS2 run. This could be in part because of the cyclical nature of supercells. As shown in the Figures 4 and 5, the four different simulations were each going through periodic strengthening and weakening. It is then possible that the "strengthening" part of the 292KS1 for instance, is stronger than the "weakening" part of the 300KS2 run.

2) In the 297KS2 run, the addition of shear changed the max 1km vorticity significantly (red dashed box in Figure 7A) but had little effect on the surface vorticity when compared to the 297KS1 run (blue dashed box in Figure 7A). This trend was different from the 295K run, indicating there is most likely a thermodynamic shift between 297K and 295K.

3) The differences in dynamic forcing between all three θ_0s when compared to the control were not expected. One would think that the 300KS2 run would have the most dynamic forcing compared to all other simulations, however, this is not what the results

show. The addition of shear to the 297K, 295K, and 293K runs produces dynamic forcing in the low-level atmosphere exceeding that of the 300KS2 run (i.e., the dashed red line is to the right of the solid red line in Figures 8A-C). This again, could be attributed to the complex and chaotic nature of supercells.

C. RECOMMENDATIONS FOR FUTURE WORK

This experiment covered a very limited selection of atmospheric initial conditions that attempted to capture environments that could sensibly be observed in the real world. As such, the specific set of conditions of low-level shear and low-level stability that create a balance between the two forcing mechanisms was elusive. Future studies that incorporate a wider range of wind and thermodynamic profiles could help discover this unique equilibrium.

Although this experiment used an analytic sounding and wind profile that previous studies have used and proven their applicability to simulate real-world environments, nothing beats the real thing when it comes to actual soundings taken from areas that produced tornadic supercells. An analysis of observations from environments near nocturnal tornadoes, and a comparison of these environments with those where supercells failed to produce tornadoes, would complement the numerical modeling experiments in this thesis.

Finally, because this experiment attempted to solve the larger question of why tornadoes still occur after dark despite an increase in low-level stability, further research could be done to determine whether nocturnal tornadoes associated with the LLJ are stronger than tornadoes that occur before the sun sets.

THIS PAGE INTENTIONALLY LEFT BLANK

LIST OF REFERENCES

Adlerman, E., and K. Droegemeier, 2005: The dependence of numerically simulated cyclic mesocyclogenesis upon environmental vertical wind shear. *Mon. Weather Rev.,* **133**, 3595–3623.

Anderson-Frey, A., Y. Richardson, A. Dean, R. Thompson, and B. Smith, 2016: Investigation of near-storm environments for tornado events and warnings. *Weather and Forecasting; Weather Forecast.,* **31**, 1771–1790.

Ashley, W., 2007: Spatial and temporal analysis of tornado fatalities in the United States: 1880–2005. *Weather and Forecasting,* **22**, 1214–1228.

Bryan, G., and J. Fritsch, 2002: A benchmark simulation for moist nonhydrostatic numerical models. *Mon. Weather Rev.,* **130**, 2917.

Bunkers, M., B. Klimowski, J. Zeitler, R. Thompson, and M. Weisman, 2000: Predicting supercell motion using a new hodograph technique. *Weather and Forecasting, Boston, MA,* **15**, 61–79.

Coffer, B. E., and M. D. Parker, 2017: Simulated supercells in nontornadic and tornadic VORTEX2 environments. *Monthly Weather Review,* **145**, 149–180.

Coffer, B. E., and M. D. Parker, 2015: Impacts of increasing low-level shear on supercells during the early evening transition. *Monthly Weather Review,* **143**, 150209132625008.

Coffer, B. E., M. D. Parker, J. M. L. Dahl, L. J. Wicker, and A. J. Clark, 2017: Volatility of tornadogenesis: An ensemble of simulated nontornadic and tornadic supercells in VORTEX2 environments. *Mon. Wea. Rev.,* **145**, 0152.

Corfidi, S., S. Corfidi, and D. Schultz, 2008: Elevated convection and castellanus: Ambiguities, significance, and questions. *Weather and Forecasting,* **23**, 1303.

Davies-Jones, R., 2002: Linear and nonlinear propagation of supercell storms. *J. Atmos. Sci.,* **59**, 3178–3205.

Du, Y., and R. Rotunno, 2014: A simple analytical model of the nocturnal low-level jet over the Great Plains of the United States. *J. Atmos. Sci.,* **71**, 3674.

Efron, B., 1979: Bootstrap methods: Another look at the jackknife. *The Annals of Statistics,* **7**, 1–26.

Gallus, W., N. Snook, and E. Johnson, 2008: Spring and summer severe weather reports over the Midwest as a function of convective mode: A preliminary study. *Weather and Forecasting,* **23**, 101–113.

Klemp, J. B., and D. R. Durran, 1983: An upper boundary condition permitting internal gravity wave radiation in numerical mesoscale models. *Monthly Weather Review,* **111**, 430–444.

Markowski, P., C. Hannon, J. Frame, and E. Lancaster, 2003: Characteristics of vertical wind profiles near supercells obtained from the Rapid Update Cycle. *Weather and Forecasting,* **18**, 1272.

Markowski, P. M., and Y. P. Richardson, 2014: The influence of environmental low-level shear and cold pools on tornadogenesis: Insights from idealized simulations. *Journal of the Atmospheric Sciences,* **71**, 243–275.

Morrison, H., 2005: A new double-moment microphysics parameterization for application in cloud and climate models. Part I: Description. *Journal of the Atmospheric Sciences.,* **62**, 1665.

Naylor, J., and M. S. Gilmore, 2014: Vorticity evolution leading to tornadogenesis and tornadogenesis failure in simulated supercells. *J. Atmos. Sci.,* **71**, 1201–1217.

Nowotarski, C. J., P. M. Markowski, and Y. P. Richardson, 2011: The characteristics of numerically simulated supercell storms situated over statically stable boundary layers. *Monthly Weather Review,* **139**, 3139–3162.

Parker, M. D., and R. Johnson, 2004: Structures and dynamics of quasi-2D mesoscale convective systems. *J. Atmos. Sci.,* **61**, 545–567.

Rasmussen, E., and D. Blanchard, 1998: A baseline climatology of sounding-derived supercell and tornado forecast parameters. *Weather and Forecasting,* **13**, 1148–1164.

Rotunno, R., and J. Klemp, 1982: The influence of the shear-induced pressure gradient on thunderstorm motion. *Mon. Weather Rev.,* **110**, 136–151.

Shapiro, A., and E. Fedorovich, 2009: Nocturnal low-level jet over a shallow slope. *Acta Geophys.,* **57**, 950–980.

Simmons, K. M., D. Sutter, and R. Pielke, 2013: Normalized tornado damage in the United States: 1950–2011. *Environmental Hazards,* **12**, 132–147.

Thompson, R. L., 2003: Close proximity soundings within supercell environments obtained from the Rapid Update Cycle. *Weather and Forecasting.,* **18**, 1243.

Thompson, R., 1998: Eta model storm-relative winds associated with tornadic and nontornadic supercells. *Weather and Forecasting,* **13**, 125–137.

Weisman, M. L., and J. B. Klemp, 1982: The dependence of numerically simulated convective storms on vertical wind shear and buoyancy. *Monthly Weather Review,* **110**, 504–520.

Weisman, M., and R. Rotunno, 2000: The use of vertical wind shear versus helicity in interpreting supercell dynamics. *J. Atmos. Sci.*, **57**, 1452–1472.

THIS PAGE INTENTIONALLY LEFT BLANK

INITIAL DISTRIBUTION LIST

1. Defense Technical Information Center
   Ft. Belvoir, Virginia

2. Dudley Knox Library
   Naval Postgraduate School
   Monterey, California